Asociación Argentina
de Mecánica Computacional

Mecánica Computacional Vol XXXV, págs. 1809-1825 (artículo completo)
Martín I. Idiart, Ana E. Scarabino y Mario A. Storti (Eds.)
La Plata, 7-10 Noviembre 2017

NUMERICAL SIMULATION OF SIPHON BREAKER OF AN OPEN-POOL TYPE RESEARCH REACTOR

Damian E. Ramajo[a], Santiago F. Corzo[a], Patricio Alberto[b], Clarisa Moscciaro[b], Maria Saez[b] and Norberto M. Nigro[a]

[a]*CIMEC Centro de Investigación de Métodos Computacionales, UNL, CONICET, FICH, Col. Ruta 168 s/n, Predio Conicet "Dr Alberto Cassano", 3000 Santa Fe, Argentina,*
damianramajocimec@gmail.com, *http://www.cimec.org.ar*

[b]*INVAP S.E., Av. Cmte. Luis Piedrabuena 4950, (R8403CPV) S.C. de Bariloche, Argentina,*
PAAlberto@invap.com.ar, *http://http://www.invap.com.ar*

Keywords: CFD, Siphon Breaker, Nuclear Reactor

Abstract. A numerical investigation of the siphon breaker of an open-pool type nuclear research reactor was performed by Computational Fluid Dynamics. The computational model was assessed by solving a siphon break line design, for which experimental and numerical data are available. The multiphase problem was solved with Volume of Fluid Method and k-epsilon for turbulence modeling. Numerical results were in very good agreement with experimental data. The siphon breaker occurrence was verified and the undershooting height, measured from the pool level to the siphon break line end as well as the liquid mass flow rate inside the main pipe were well captured. The implemented model showed to be reliable for assessing this kind of passive safety systems.

LIST OF SYMBOLS

γ: Phase fraction []
U: Velocity [m/s]
p: Pressure [Pa]
p_{rgh}: Pressure corrected by the hydrostatic column [Pa]
t: Time [s]
ρ: Density [kg/m^3]
μ: Dynamic viscosity [Pa s]
τ: Stress tensor [N/m^2]
I: Identity matrix
k: Turbulent kinetic energy [m^2/s^2]
ε: Turbulent dissipation rate [m^2/s^3]
σ: Surface tension coefficient [N/m]
g: Gravitational acceleration [m/s^2]
S: Mean rate stress tensor
x: Position vector [m]
D_s: Characteristic grid size [m]

Subscripts:

γ: Phase index
l: Liquid phase
g: Gas phase
r: Relative value
w: Wall
eff: Effective

Acronyms:

CFD: Computational Fluid Dynamics
GAMG: Geometric Algebraic Multi-Grid
MULES: Multid. Univ. Limiter with Explicit Sol
RANS: Reynolds-averaged Navier-Stokes
SGS: Symmetric Gauss-Seidel
VOF: Volume of Fluid
SBL: Siphon Break Line
SBH: Siphon Break Hole
SBV: Siphon Break Valve
NPSH: Net Positive Suction Head

1 INTRODUCTION

Low power nuclear research reactors are developed for a variety of applications such as research of new fuels, new materials, core configurations, teaching, radioisotopes production and specific medical treatments, among others. Even though the purpose of the research reactor is to use neutrons, the heat generated by the core have to be removed and the core flow have to be guaranteed by a cooling system. The open-pool type research reactors are widely used because of versatility in which the water is the coolant and also the moderator. The pool water also behaves as a shedding barrier for many radio-nuclides resulting from the reactor core or the spent fuel. One security characteristic of them is that the natural circulation have be enough to remove the decay power and keep cooled the core if the primary cooling pump turned off. In

these reactors the pool water is the ultimate heat sink and a large pool is the heart of the nuclear safety Seo et al. (2012). Consequently, to ensure a minimum water level or water inventory is a crucial requirement for the reactor design. The reactor pool has to be designed in a safety class and the lowest pipe suction have to be above of the reactor core to avoid complete voiding under a cooling pipe break. However, it is not always possible because a Net Positive Suction Head (NPSH) should be available at the coolant pump inlet. Therefore, in practice the coolant pipe inlet is placed below the secure minimum liquid level. Hence, if a pipe break occurs below to the reactor core level, the pool water can be drained through a siphon effect and the decay heat could no longer be removed by natural circulation. Under this possible scenario, a passive siphon breaker system should be installed to limit the water drainage under a Loss of Coolant Accident (LOCA). Most cooling pipes are large in diameter to reduce the pressure drop across the circuit, and consequently the pump power and the *NPSH* required. However, in this situations it should be more difficult to break a siphon effect than for small pipe diameters.

Two kind of passive siphon breakers are normally used: the siphon break lines (SBL) and the siphon break holes (SBH). The SBL consists on a small size pipe. In same designs one of the pipe ends (pipe inlet) is submerged into the open-pool reactor but in other designs this pipe end is open to the air. The other pipe end (pipe outlet) is connected to a top U-bend placed at the outlet side of the coolant pipe. On the other hand, the SBH is a small hole drilled in the inlet side of the coolant pipe. During normal operation, both the inlet end of the SBL (for same designs) as well as the SBH are completely submerged in the pool. Furthermore, the SBL can have valves to restrict the by-pass flow.

Perhaps the first study concerning to siphon breakers in nuclear reactors was from McDonald and Marten (1959). However, they worked with high-temperature sodium flows and small size pipe systems. Therefore, the conclusions they arrived can not be easy extrapolated to water-coolant flowing through large size pipe systems. Posteriorly, Hirano and Sudo (1986) numerically studied the open-pool research reactor JRR-3 by means of a code based on the so-called one-dimensional node-and-junction method. They simulated the thermal hydraulics behavior of the reactor under LOCA events. In order to prevent complete pool water discharge, two siphon break valves (SBV) and a SBH were incorporated in the primary cooling loop of U-bends to break the siphon effect at the core outlet and inlet sides. The SBV were designed to be opened when the pool water level gets below a certain value. It was expected that air starts to enter into the primary cooling loop through the SBV and the SBH once the pool level reaches the siphon break level. Although the researchers remarked the importance of the siphon breakers to isolate the water pool under a LOCA event, they focused into understand the transient from the forced convection core cooling to the natural circulation core cooling. Therefore, they assumed that the siphon breakers worked as expected. After that, Neil and Stephens (1993) experimentally studied the hydraulic characteristics when siphon effect is broken. Although the huge amount of data recovered, it was not enough to cover the range of conditions that take place in research reactors. Therefore, they do not provide a practical method to calculate and design siphon breakers for research reactors.

Up to the moment, siphon breaker studies have concerned mainly to experimental facility tests. Seo and co-workers had been studying siphon breakers since 2011. The first contribution from they discussed about the kind of breaker required for the different nuclear reactors. Seo et al. (2011) reported that, for upward reactors (the flow cross the core from the bottom to the top) a passive SBH or SBL can be installed both in the inlet and the outlet pipes of the reactor. On the other hand, for downward reactors (the flow cross the core from the top to the bottom) a SBH or SBL can be installed at the inlet but a SBV is required at the outlet, in order

to guarantee the required NPSH. Seo et al. (2012) built a real-scale facility to investigate the siphon effect on the Jordan Research and Training Reactor (JRTR). The experimental facility was a water cubic open-pool of around 60 m^3 and a coolant pipe size of 16 inch diameter, with several elbows. They simulated a LOCA of 10 inch in the main pipe and measured the surface velocity, the pressure in several positions in the main pipe and the pool level evolution in order to quantify the undershooting (height from the pool level to the SBL end). Several SBL diameters were experimentally studied (1, 1.5, 2 and 2.5 inch) and some of them were also simulated by Computational Fluid Dynamics (CFD). They performed simulations with Fluent using the Volume of Fluid (VOF) method as well as the Euler-Euler two-phase model. Although the results from Seo et al. (2012) were not in good agreement with experimental data, they concluded that the VOF method over predicted the undershooting, whereas the Euler-Euler method under predicted it. They also found that discrepancies became larger for SBL of small diameter. Then, Park et al. (2014) carried out additional numerical tests to determinate the influence of modeling the pool-water free surface with different methods and different surface tension coefficients, but they found that had negligible influence on the siphon effect break.

Latterly, Kang et al. (2013) performed experimental tests over the same facility but for other configurations. they reduced the SBL diameter up to 0.5 inch and increased the LOCA rupture size up to 6 and 8 inch. They also carried out tests using SBL, SBH and combining both systems. For tests with only SBL, the time until siphon effect broken increased from 45 sec to more than 150 sec when the SBL size (ϕ_b) was reduced from 2.5 to 1.5 inch. The undershooting height h_{under} followed a similar behavior; It quickly increased by reducing ϕ_b. e.g., for a rupture of 10 inch and ϕ_b = 2.5, 2.0 and 1.5 inch, the h_{under} were 34 mm, 77 mm and 153 mm, respectively. Finally, for the smaller SBL (ϕ_b = 1.0 and 0.5 inch), the siphon effect never broken. and the water pool was completely empty. On the other hand, the incorporation of the SBH along with the SBL reduced the undershooting height up to 30 mm, 42 mm and 85 mm. Moreover, the siphon effect was broken for ϕ_b = 1.0, although the undershooting height was more than 2800 mm.

In 2014 Kang et al. (2014) continued testing different rupture LOCA sizes (12, 14 and 16 inch) and SBL sizes (ϕ_b = 3, 4, 5 and 6 inch) and determined that the undershooting height is largely depending on the SBL size but almost independent of the rupture size.

The large amount of experimental data obtained by Seo et al. (2012), Kang et al. (2013) and Kang et al. (2014) leads to Lee and Kim (2017) to develop an ad-hoc code to design and calculate siphon breakers. The code accounts for a set of basic constructive parameters and allows quickly estimate the undershooting-height evolution as well as the pressure in some points and the coolant mass flow. Despite the usefulness of this code, it only solves basic rectangular pool configurations. That is, it does not consider the core configuration. Furthermore, the coolant circuit layout is only restricted to pipes and elbows. Considering the importance of the siphon breakers, the code only should be considered as an initial estimation and the final design should be assessed by more reliable methods.

This paper address with the simulation by CFD of one of the experimental and numerical tests carried out by Seo et al. (2012) in order to enhance the numerical estimations and to demonstrate the suitability and potentiality of the CFD.

2 MATHEMATICAL FORMULATION

The mathematical background presented below is based on the Volume Of Fluid (VOF) solver `interFoam` from OpenFOAM-3.0.1© (Open Field Operation and Manipulation). The VOF method was proposed by Hirt and Nichols (1981) and relies on the definition of an indi-

cator function, which allows knowing whether the computational cell is filled by one fluid, by the other or by a mix of them. This is accomplished by the phase fraction γ, which can take values within the range $0 \leq \gamma \leq 1$, where the extreme values of 0 and 1 are associated to cells in which only one phase is present. In this case, $\gamma = 0$ for air and $\gamma = 1$ for water. A concise explanation of the method can be found in Berberovic et al. (2010). One of the critical issues using VOF is the conservation of the phase fraction γ. This is specially the case in flows with high density ratios, such as the current system. In these cases, small errors in γ may lead to significant differences in the estimation of the physical properties of the mixture. Furthermore, accurate calculation of the phase fraction distribution is crucial to get thin and smooth interfaces required to evaluate the curvature an the consequent surface tension efforts and pressure gradients through the interface. The interface is typically smeared over a few grid cells and is therefore highly sensitive to grid resolution. In the conventional VOF method the transport equation γ is solved simultaneously with the continuity and momentum equations. It is not a simple task to assure boundedness and conservativeness of the phase fraction. The governing equations for unsteady incompressible flow are the equation of continuity, the transport of γ and the Navier-Stokes equation:

$$\nabla \cdot \mathbf{U} = 0 \tag{1}$$

$$\frac{\partial \gamma}{\partial t} + \nabla \cdot (\mathbf{U}\gamma) = 0 \tag{2}$$

$$\frac{\partial (\rho \mathbf{U})}{\partial t} + \nabla \cdot (\rho \mathbf{U}\mathbf{U}) = -\nabla p + \nabla \cdot \tau + \rho \mathbf{g} + \sigma \kappa \nabla \gamma \tag{3}$$

where $\mathbf{U}$ represents the velocity field shared by the two fluids throughout the flow domain, γ is the phase fraction and τ is the deviatoric viscous stress tensor, ρ is the density, p the pressure and $\mathbf{g}$ the gravitational acceleration. σ is the surface tension coefficient and κ is the local curvature of the free surface. The last term in Equation 3 represents the surface tension force and was proposed by Brackbill et al. (1992). The curvature κ is defined as:

$$\kappa = -\nabla \cdot \left(\frac{\nabla \gamma}{|\nabla \gamma|}\right) \tag{4}$$

In OpenFOAM a modified approach is used; The fluid velocity $\mathbf{U}$ is proportional to the velocity of both phases whereas the interface compression velocity is equal to the relative velocity amount them ($\mathbf{U_r}$):

$$\mathbf{U} = \gamma \mathbf{U_l} + (1-\gamma)\mathbf{U_g} \qquad \mathbf{U_r} = \mathbf{U_l} - \mathbf{U_g} \tag{5}$$

where $\mathbf{U_l}$ and $\mathbf{U_g}$ are the liquid and the gas velocities, respectively. Then, it is possible to write the γ equation (Eq. 2) in terms of $\mathbf{U_r}$:

$$\frac{\partial \gamma}{\partial t} + \nabla \cdot (\mathbf{U}\gamma) + \nabla \cdot (\mathbf{U_r}\gamma(1-\gamma)) = 0 \tag{6}$$

Summarizing, two immiscible fluids are considered as one fluid throughout the domain and its physical properties are calculated as weighted averages based on the volume fractions. Then,

single-phase properties are obtained everywhere except in the interface, where mixed properties are calculated:

$$\rho = \rho_l\gamma + \rho_g(1-\gamma) \qquad \mu = \mu_l\gamma + \mu_g(1-\gamma) \tag{7}$$

For the *interFoam* solver, OpenFoam defines a modified pressure named p_{rgh}, which is defined as:

$$p_{rgh} = p - \rho\mathbf{g}\cdot\mathbf{x} \tag{8}$$

where $\mathbf{x}$ is the position vector. Finally, for Newtonian and incompressible fluids the strain rate tensor S is linearly related to the stress tensor ($\tau = 2\mu\mathbf{S}$ - $2\mu(\nabla\cdot\mathbf{U})\mathbf{I}/3$ with $\mathbf{S} = 0.5[\nabla\mathbf{U} + (\nabla\mathbf{U})^T]$). Therefore, the momentum equation can be rearranged to get:

$$\begin{aligned} &\frac{\partial(\rho\mathbf{U})}{\partial t} + \nabla\cdot(\rho\mathbf{U}\mathbf{U}) - \nabla\cdot(\mu\nabla U) = \\ &-\nabla p_{rgh} - \mathbf{g}\mathbf{x}\cdot\nabla\rho + \nabla\cdot(\mu(\nabla\mathbf{U})^T) + \sigma\kappa\nabla\gamma \end{aligned} \tag{9}$$

Summarizing, the present mathematical model accounts for the continuity equation 1, the phase fraction equation 6 and the momentum equation 9. Finally, the ensemble averaging leads to the Reynolds-averaged Navier-Stokes (RANS).

The standard RANS k-ε model with logarithmic wall law was chosen to obtain the turbulent viscosity μ_t through two additional equations for the transport of the turbulent kinetic energy k and the turbulent dissipation rate ε:

$$\frac{\partial\rho k}{\partial t} + \nabla\cdot(\rho kU) = \nabla\cdot\left(\frac{\mu_{eff}}{\sigma_k}\nabla k\right) + 2\mu_t S:S - \rho\varepsilon \tag{10}$$

$$\frac{\partial\rho\varepsilon}{\partial t} + \nabla\cdot(\rho\varepsilon U) = \nabla\cdot\left(\frac{\mu_{eff}}{\sigma_\varepsilon}\nabla\varepsilon\right) + C_{1\varepsilon}2\mu_t S:S - C_{2\varepsilon}\frac{\rho\varepsilon^2}{k} \tag{11}$$

where $\mu_{eff} = \mu + \mu_t$ the effective viscosity. Then, μ_t is defined as follows:

$$\mu_t = \rho C_\mu\frac{k^2}{\varepsilon} \tag{12}$$

The model constants were by default $C_u = 0.09$, $C_{1\varepsilon} = 1.44$, $C_{2\varepsilon} = 1.92$, $\sigma_k = 1.0$ and $\sigma_\varepsilon = 1.3$.

3 COMPUTATIONAL MODEL

3.1 TEST GEOMETRY AND COMPUTATIONAL DOMAIN

As mentioned, there are two typical siphon beakers: SBL and SBH. Experimental data for each one and for the combination of them are available in literature. Due to the long time required for simulations, in this paper only the 2.5 inch ($\phi_i n$ = 69 mm) SBL with a 10 inch LOCA was evaluated. Figure 1 shows a draw of the test configuration and the main geometrical parameters. The open-pool reactor is a cube of 4 m wide $\times$ 3.7 m depth $\times$ 4 m height with a total volume closer to 60 m^3. the total height from the top of the open-pool to the center line of the discharge mouthpiece at the bottom is 12.250 m. The water leaves the pool through an outlet at the bottom left of the pool. The main pipe line is 16 inch in diameter ($\phi_i n$ = 390.6

mm). It is made of straight pipes, five large radius elbows and one outlet mouthpiece with a contraction from 16:10 inch ($\phi_i n$ = 254.4 mm) to finally discharge into an open pool. The main line has a bottom U-bend shape below the pool and a top U-bend shape close to the top of the pool.

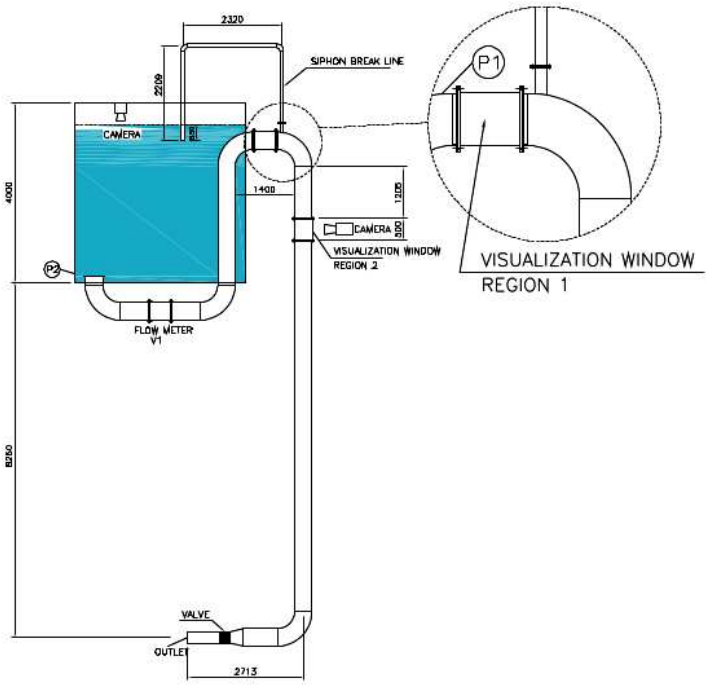

Figure 1: View of the test geometry with the main constructive parameters (Courtesy of Seo et al. (2012)).

As showed in Figure 1, the left extreme of the breaker line (SBL inlet) is submerged in the water pool and the right extreme (SBL outlet) is connected to the top U-bend of the main line. It should be remarked that some constructive details, such as the exact location of the connection point between the SBL outlet and the main pipe or the length of the 10 inch straight pipe at the outlet of the line are not reported in the several papers concerning to this facility. However, the more important geometry parameters are known.

Taking advantage of the symmetry of the installation, only a half of the full geometry was simulated. Figure 2 shows the external and auxiliary surfaces required to define the geometry and to perform local refinement around the main line and the SBL. Both lines were completely meshed with structured grids. Therefore, a set of auxiliary surface were needed.

Figure 3 displays details of the mesh. In picture *a* a general view of the pool water is shown. As noted, the SBL inlet and the discharge connection were specially refined. The pool water was meshed with triangles at the surface and with hexaedral elements in the core to reduce the total amount of cells (see picture *b*). The transitions between elements was carefully achieved because of the large aspect ratio. e.g. the elements size near the SBL wall was 0.5 mm whereas the maximum element size in the pool reached 60 mm (see picture *c*). The last picture (*d*) shows the refinement around the top U-bend. In order to merge the structured grids, a part of the elbow of the main line was meshed with unstructured tetrahedral cells. Note that the thickness of the SBL and the main duct inside of the pool were represented in order to separate the inner duct cells from the outer ones, thus allowing to use very different cells sizes in both sides. The overall mesh had 3.629.322 elements, with 1.267.221 tetrahedral, 1.393.314 hexahedral,

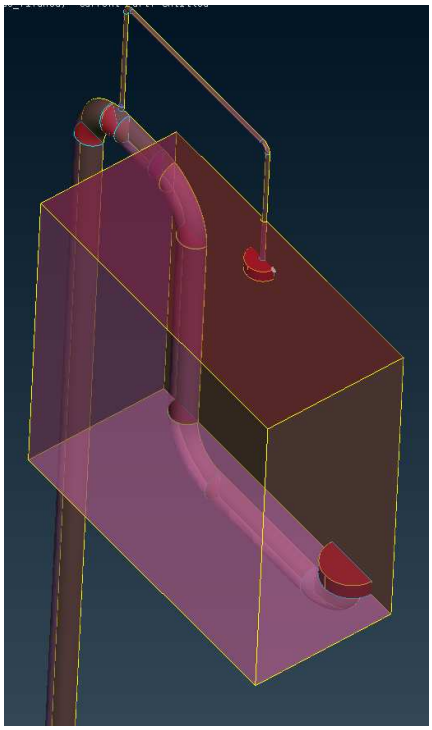

Figure 2: View of the test geometry with the main constructive parameters.

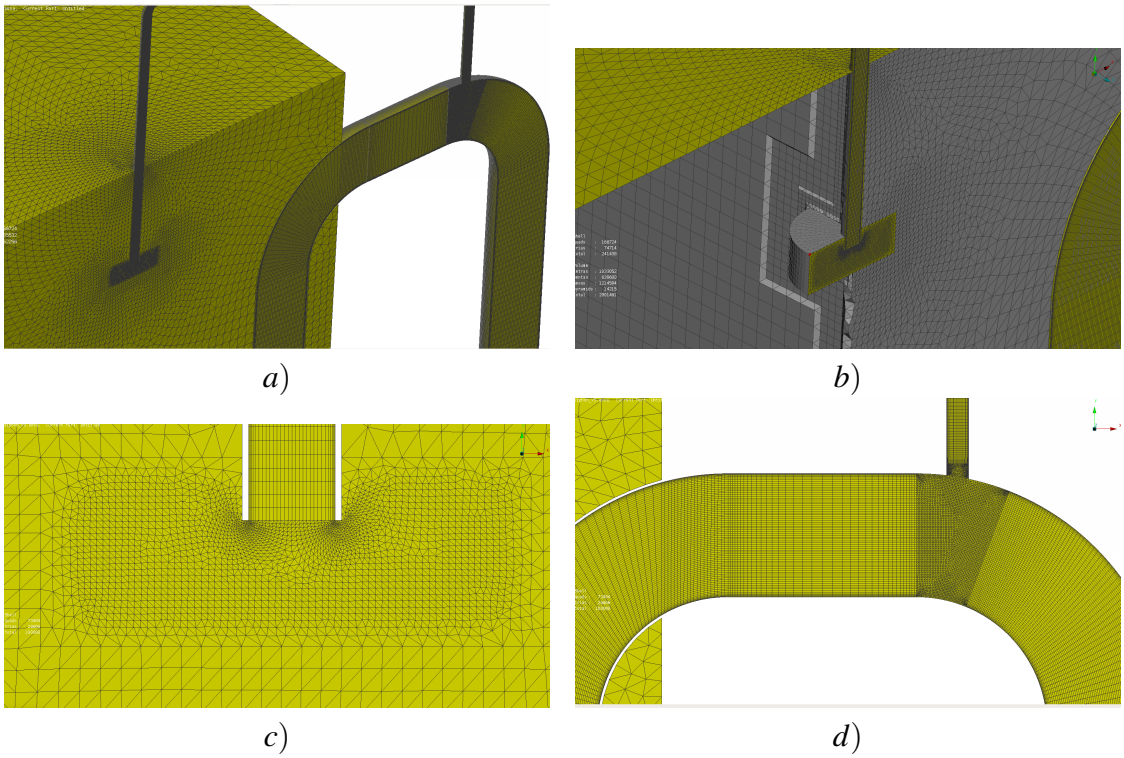

Figure 3: View of the test geometry with the main constructive parameters.

930.433 pentahedral and 38.354 pyramidal elements. The quality of the mesh was acceptable: the maximum skewness was 1.35 and the average non-orthogonality was 12.45°. although 5 faces had more than 70°. In order to keep bounded the y^+ parameter, the thickness of the first layer elements were 0.57 mm and 1.1 mm for the SBL and the main duct, respectively. The y^+ during the first simulation seconds (when only water was flowing) was around 100 for the main line and less than 50 for the SBL. These are suitable values when standard logarithmic law is employed.

The boundary conditions were no slip wall (*fixedValue* U = 0) for the pool and pipe walls and *symmetry* for the split plane. Finally, atmospheric conditions were imposed for the roof of the pool through a constant pressure condition for p_{rgh} (*totalPressure*) $p_{rgh} = 1 \times 10^5 Pa$. The velocity condition was of type inlet/outlet (*pressureInletOutletVelocity*). Regarding the outlet of the main line, a dynamic pressure condition (*prghPressure*) for p_{rgh} was used to hold the pressure at a constant value ($p = 1 \times 10^5$) while the pool water is emptying. It is needed in the outlet because of ρ of the flow crossing the outlet changes in time and that affects the p_{rhg} estimation (see Equation 8).

3.2 NUMERICAL SETTINGS

The transient simulation was carried out in distributed parallel computing in 64 processors in a beowulf cluster (Seshat) using 16 nodes (Intel(R) Xeon(R) CPU E5-1620 v2 @ 3.70GHz -1 CPU x 4 cores) with Infiniband (QDR 40 Gbps).

Adjustable time step with maximum Cu and maximum interface Cu of 12.0 and 4.0 was employed. That guaranteed stability as well as accuracy keeping bounded the interface. In order to fulfill this limits, the adjustable time step was around 6×10^{-5} sec in the most of the time. That allows to get local and global continuity errors lower than $1x10^{-11}$ and $5x10^{-15}$, respectively. However, due to these restrictive conditions the simulation of 27.6 sec demanded around 50 days. The main setting parameters are tabulated in Table 1

To use Maximum Courant around 12.0 was able by increase up to 10 the sub cycling number to increase the accuracy of the γ solution.

4 RESULTS AND DISCUSSION

For the simulated case the experimental data indicated that the siphon effect is broken after 25 sec or 30 sec (depending on the initial pool level). The available experimental data for comparison were the undershooting height and the differential pressure in time in the downward direction of the vertical part of the main pipe in Kang et al. (2014). However, for the former the exact location of the measurement points was unavailable. Regarding the numerical data, Seo et al. (2012) also reported the undershooting results as well as the time-evolution of the absolute pressure near the SBL discharge.

Figure 4 shows a set of pictures of the volume fraction of water at six times (5, 10, 15, 20 sec, 22 and 27.6 sec after the beginning of simulation). As noted, in picture *a* (5 sec) the SBL is completely full of water and there is a by-pass flow from the pool to the top U-bend. In picture *b* (10 sec) the pool level is just below to the SBL inlet and air is entering to the main pipe, but some water is still in the SBL. After 15 sec (picture *c*) the SBL is full of air and large amount of air is already entering to the main line. In the main line the phases are largely segregated and the interface among them is well defined around the top U-bend. Downstream there, large air clusters are identified in the vertical part of the pipe and smaller structures can be identified around the bottom elbow. In picture *d* (20 sec) almost the whole vertical duct is full of air,

Term	OpenFOAM terminology	Method/Scheme
$\frac{\partial}{\partial t}$	ddtSchemes	Euler
$\nabla\cdot()$	gradSchemes	Gauss Linear
$\nabla\cdot(\nabla..)$	laplacianSchemes	Gauss linear limited 0.5
$\nabla\mathbf{U}$	div(rhoPhi,U)	Gauss upwind
∇k	div(phi,k)	Gauss upwind
$\nabla\varepsilon$	div(phi,epsilon)	Gauss upwind
$\nabla\alpha$	div(phi,alpha)	Gauss vanLeer
$\nabla\alpha$	div(phirb,alpha)	Gauss vanLeer
$\nabla\cdot(\mu\nabla U)$	div(((rho*nuEff)*dev2(T(grad(U)))))	Gauss linear
	interpolationSchemes	Linear
	snGradSchemes	limited 0.5
Eqn.	Solver	Abs. tol.
γ	MULES	1×10^{-8}
	nAlphaCorr	1
	nAlphaSubCycles	10
	alphaOuterCorrectors	yes
	solver	symGaussSeidel
p_{rgh}	GAMG	1×10^{-8}
	smoother	DIC
U,k,ε	smoothSolver symGaussSeidel	1×10^{-8}
PIMPLE	Momentum pred.	yes
	nOuterCor, nCor, nNonOrthCor	3,2,2

Table 1: Solvers and settings description.

although a thin water layer falls over the left of the pipe. In picture *e* (22 sec) it can be observed how the water-air interface around the top U-bend moves toward the left. Now negligible water is flowing through the vertical pipe. Finally, picture *f* (27.6 sec) shows the end of the simulation. The velocity in the main pipe has become negative (reverse flow) because a fraction of the liquid remaining in the top U-bend is returning to the pool.

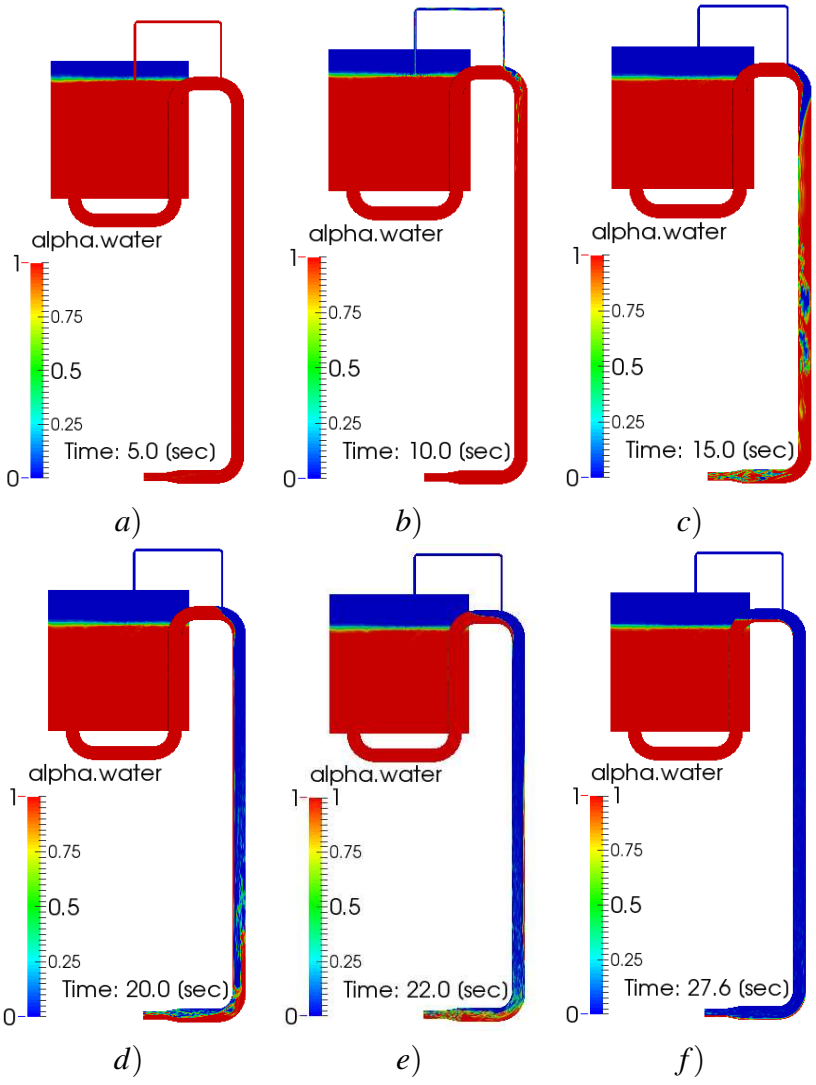

Figure 4: Volume fraction of water over the symmetry plane at six times. a): 5 sec. b): 10 sec. c): 15 sec. d): 20 sec e): 22 sec. f): 27.6 sec.

Figure 5 *a* shows the evolution of the surface velocity in the main line measured in the bottom U-bend (such as in the experiments). The water was motionless at the beginning of simulation, but it quickly accelerated up to around 5 m/s after the first 5 sec. Then it remained almost constant until t = 10 sec. Then, the air started to fill the main line and the velocity fell almost linearly until to reach 1 m/s at 20 sec. After that, the velocity continued reducing very slowly.

In Figure 5 b) is drawn the dependency of the velocity with the pool level. This is a more useful way to show the results because it is independent of the initial pool level. Is is clear that the velocity starts to decrease once the pool level get lower than the SBL inlet height (h = 3.34 m). Figure 5 c) displays the undershooting height vs time. Note that undershooting increases

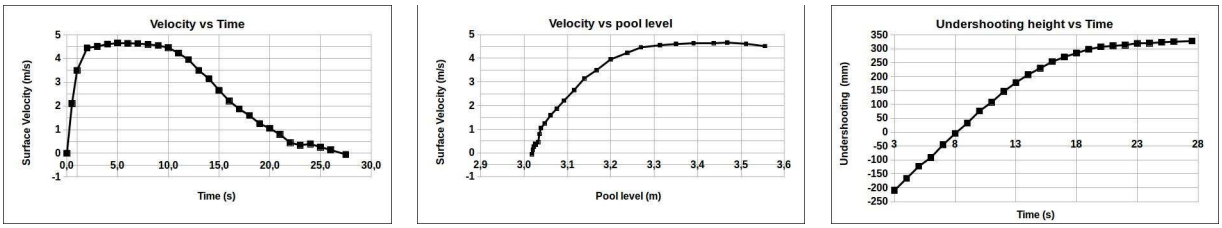

a) *b*) *c*)

Figure 5: a): Surface velocity in the main line vs time. b): Surface velocity in the main line vs pool height. c) Undeshooting vs time

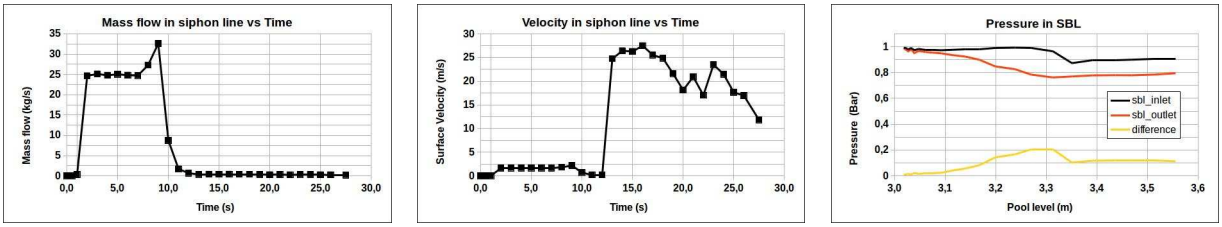

a) *b*) *c*)

Figure 6: Flow through the SBL. a): Mass flow vs. time b): Velocity vs. time. c): Pressures in the SBL vs pool level

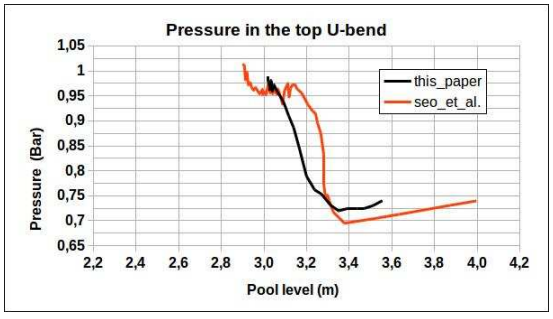

Figure 7: Pressure in the top U-bend. Comparison with the numerical results (Euler-Euler model) from Seo et al. (2012)

Case	Code	Multiphase model	Turbulence model	Undershooting	Error
This paper	OpenFOAM	VOF	k-ε	327mm	3.8%
Seo et al. (2012)	Fluent	VOF	SST	830mm	144%
	Fluent	Euler-Euler	SST	450mm	32%

Table 2: Comparison between this paper and Seo et al. (2012) results.

linearly during the first 13 sec to becomes asymptotic after t = 20 sec. The pool level reduces 500 mm between t = 3 sec and 20 sec, but it only reduces 17 mm during the last 7 sec. The final undershooting height is 327 mm, which is in very good agreement with the experiment (340 mm). That means that the relative error is only 3.8%.

Table 2 compares the current results with those obtained by Seo et al. (2012). They found undershooting heights of 450 mm and 830 mm using the Euler-Euler multiphase and the VOF models, respectively and the relative errors were very higher. Therefore, the current result represents a great improvement with respect to the previous ones.

The Figure 6 shows the mass flow (*a*) and the surface velocity (*b*) across the SBL outlet. Furthermore, the pressures at the inlet (black line), the outlet (red line) and the pressure difference (yellow line) along the SBL are drawn in picture *c*. As noted, the water mass flow is established after the first two seconds and it remains almost constant until the air starts to enter to the SBL. The mass flow of water is around 25 kg/s, which is around 5% of the total mass flow that flows through the main line during because of the siphon effect. After the first 7 sec, the air starts to enter to the pipe and consequently the frictional pressure drop through the SBL falls down. Accordingly, the water-air mixture accelerates and the mass flow increases up to 32 kg/s. Then, the air starts to cross the SBL outlet and the mass flow quickly reduces. Finally, a mass flow of air ranging between 0.3 and 0.4 kg/s is established during the subsequent 14 sec. Regarding the pressures, the picture *c* shows the pressures at the inlet and outlet of the SBL. In this case, the measurement point were placed two diameters downstream and upstream of the inlet and outlet, respectively. As noted, at the beginning, which corresponds to the right in the graphic, the inlet pressure is less than the atmospheric, but it rise ups once the pool level fall down below the SBL inlet. Similarly,the pressure at the SBL outlet remains almost constant 0.3 Bar below the atmospheric and slowly recovers the atmospheric value when the air starts to enter to the main line.

Unfortunately, few experimental data are available for the current case. However, numerical results for the pressure in the top U-bend were reported by Seo et al. (2012) with the Euler-Euler model. Figure 7 compares the results from Seo et al. (red line) with our simulation (black line). As noted, our simulation was started from a lower pool level and finished before. However, the minimum pressures seem to be similar in both cases.

Figure 8 a) shows the velocity over the symmetry plane at different instants. In Picture *a* (5 sec) the SBL is full of water and the velocity is around 3 m/s. The local acceleration of the flow around the inner curve of the elbows is already established. No significant changes between Picture *a* and *b* are found upstreams of the top U-bend. However, in Picture *b* the air is flowing across the SBL and the velocity through it is higher than the bar scale limit. Picture *c* shows a completely different view. The velocity upstream the top U-bend has been reduced below 3 m/s and flow moves slowly at the middle of the vertical pipe because of the presence of air clusters (see Figure 4). Finally, in Picture *d* the main line velocity upstreams the top U-bend has been reduced below 1 m/s. The air continues entering through the SBL outlet with a high velocity and the maximum velocity in the vertical pipe corresponds with the left side wall where liquid is still falling.

Figure 9 shows the velocity magnitude and vectors around the SBL discharge at four times. Despite the color bar limits are the same for all pictures, the air velocity is higher for picture *a* (20 sec), with a maximum value around 60 m/s. However, two seconds later the velocity reduced to a half. As noted, when the air jet impacts to the free surface it splits in two: The main jet flows downstream with the water, while a secondary jet flows opposite to the water stream. Despite the siphon is broken at 27.6 sec, the air do not stop immediately and it remains

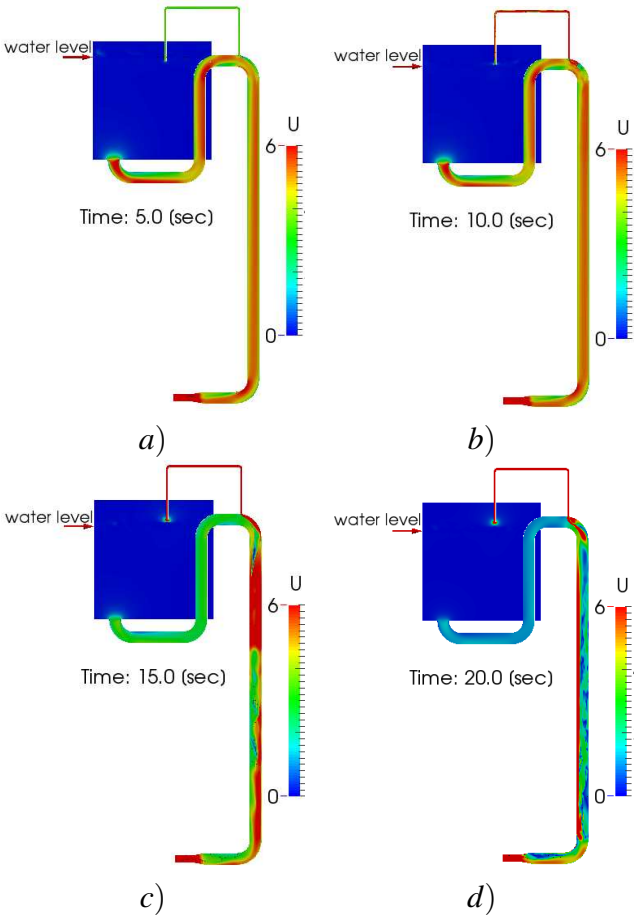

Figure 8: Velocity U over the symmetry plane at four times. a): 5 sec. b): 10 sec. c): 15 sec. d): 20 sec

flowing through the SBL with velocities around 25 m/s.

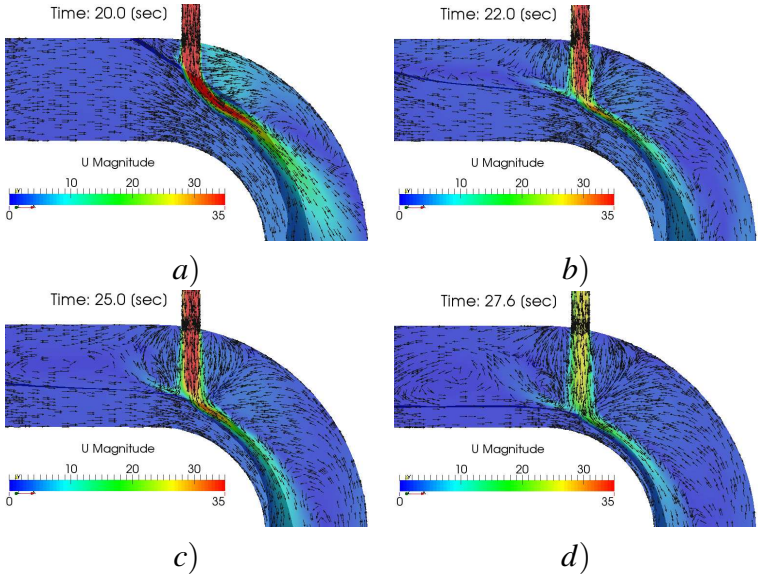

Figure 9: Velocity magnitude and vectors over the symmetry plane around the siphon discharge at four times. a): 20 sec. b): 22 sec. c): 25 sec. d): 27.6 sec

The Figure 10 also shows the effect of the air jet over the free surface producing a cavity on it. This allows to think that the location of the SBL outlet could have influence on the efficiency of the SBL.

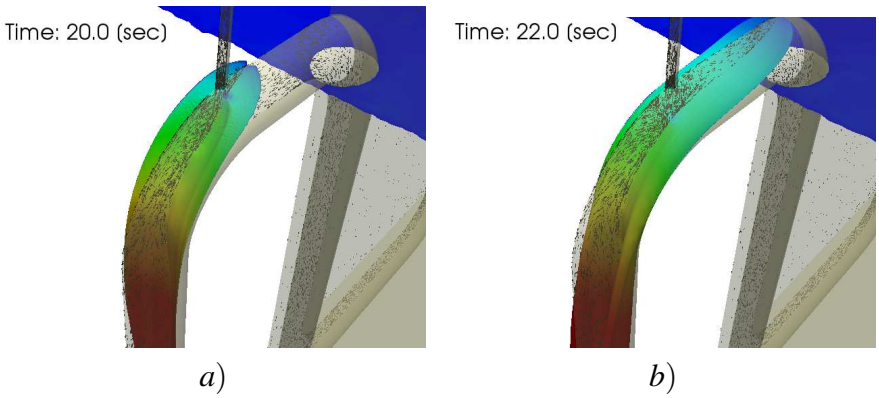

Figure 10: Velocity magnitude and vectors over the symmetry plane around the siphon discharge at four times. a): 20 sec. b): 22 sec.

5 CONCLUSIONS

This paper addressed with the multiphase simulation of the siphon-effect break in nuclear engineering applications by means of computational fluid dynamics. The numerical model was validated against experimental data from a real-scale facility finding very good agreement, thus highlighting the potentiality of the numerical method to assess this kind of safety reactor systems. The following ideas are highlighted:

The Volume of Fluid (VOF) method combined with the RANS k-ε model showed to be suitable for solving these multiphase problems despite high mesh requirements of VOF method. That could be explained because the flow is mainly stratified and the inertial effects could be dominant over the interface forces. The system is mostly single-phase in the whole of the domain, and the free surface is well defined. In this context, the VOF method recovers the exact form of the single-phase Navier-Stokes equation in almost every where.

The results from the current computational model were in very good agreement with experimental data. The relative error for the undershooting height -the main safety parameter- were 3.8%. The numerical simulations from other authors were very inaccurate with errors around 32%.

ACKNOWLEDGEMENTS

The authors would like to thank Universidad Nacional del Litoral (CAI+D 2016 PIC 50420150100067LI) and Agencia Nacional de Promocion Cientifica y Tecnologica (PICT 2013-830 and PICT 2016-2908)

REFERENCES

Berberovic E., Roisman I., Jakirlie S., and Tropea C. Computational study of hydrodymanics and heat transfer associated with a liquid drop impacting a hot surface. In *Computational Fluid Dynamics 2010, Springer*. 2010.

Brackbill J., Kothe D.B., and Zemach C. A continuum method for modeling surface tension. *Journal of computational physics*, 100(2):335–354, 1992.

Hirano M. and Sudo Y. Analytical study on thermal-hydraulic behavior of transient from forced circulation to natural circulation in jrr-3. *Journal of Nuclear Science and Technology*, 24(4):352–368, 1986.

Hirt C. and Nichols B. Volume of fluid (vof) method for the dynamics of free boundaries. *Journal of computational physics*, 39(2):201–225, 1981.

Kang S., Ahn H., Kim J., Joo H., Lee K., Seo K., Chi D., Yoon J., Jeun G., and Kim M. Experimental study of siphon breaking phenomenon in the real-scaled research reactor pool. *Nuclear Engineering and Design*, 255:28–37, 2013.

Kang S., Lee K., Lee G., Kim S., Chi D., Seo K., Yoon J., Kim M., and Park J. Investigation on effects of enlarged pipe rupture size and air penetration timing in real-scale experiment of siphon breaker. *Nuclear Engineering and Technology*, 46:817–824, 2014.

Lee K. and Kim W. Development of siphon breaker simulation program for investing loss of coolant accident of a research reactor. *Annals of Nuclear Energy*, 101:49–59, 2017.

McDonald J. and Marten W. A siphon break as a blocking valve. *Atomics International*, 1959.

Park H., Seo K., Kim S., and Chi D. Cfd analysis of siphon break in a research reactor. *Transactions of the Korean Nuclear Society Spring Meeting*, pages 1–2, 2014.

Seo K., Kang S., Kim J., Lee K., Jeong N., Chi D., Yoon J., and Kim M. Experimental and

numerical study for a siphon breaker design of a research reactor. *Annals of Nuclear Energy*, 50:94–102, 2012.

Seo K., Lee K., Yoon H., and Jeong N. Estimation on a siphon breaker type of a research reactor. *Transactions of the Korean Nuclear Society Spring Meeting*, pages 103–104, 2011.